Thermo-Optically Tunable Silicon AWG With Above 600 GHz Channel Tunability

Yan Yang, Xiaonan Hu, Junfeng Song, Qing Fang, Mingbin Yu, Xiaoguang Tu, Guo-Qiang Lo, *Senior Member, IEEE*, and Rusli, *Senior Member, IEEE*

***Abstract*— With the ever-increasing demand for small channel spacing in the dense wavelength division multiplexing technology, and the wavelength shift arising from the fabrication dimensional sensitivity of the silicon optical communication devices, wavelength tuning methods for silicon multiplexer/demultiplexer are therefore of great interest. Thermo-optically tunable silicon arrayed waveguide grating (AWG) multiplexer/demultiplexer using TiN heater has been demonstrated for the first time. Reduced impact of fabrication nonuniformity on the AWG effective refractive index is achieved through the waveguide design. Uniform heating is achieved by the heater design, which is analyzed by thermal distribution simulation. Above 600 GHz channel tunability has been demonstrated by simulation and experiment.**

***Index Terms*— Integrated optics, arrayed waveguide grating (AWG), thermo-optic (TO) effect.**

I. Introduction

ARRAYED waveguide gratings (AWG) have become increasingly popular as multiplexers/demultiplexers (MUX/DeMUX) for wavelength-division-multiplexing (WDM) applications [1]–[3]. This is due to the fact that AWG-based devices have been proven to be capable of multiplexing/demultiplexing a high number of channels [2], [3]. The ever-increasing demand for bandwidth in optical communication networks has increased the interest for dense-wavelength-division-multiplexing (DWDM) technology. This demand requires high-performance AWG wavelength MUX/DeMUX with small channel spacing [4], [5]. The designed peak wavelength of AWGs with small channel spacing is more vulnerable to the wavelength shift/drift. Therefore, methods of stabilizing and tuning, such as precise positioning of AWGs on the ITU grid, or compensating for optical wavelength drift, are of great interest. Tunable AWGs based on silica [5], InP [6]–[9], and polymer [10], [11] have been reported. However, tuning method for silicon AWG was not reported yet.

CMOS-compatible silicon photonics is becoming a promising technology to realize high performance photonics-CMOS integration system. Silicon AWG is a critical and extensively used optical component in the silicon optical communication networks. One of the major issues in using a high-index contrast platform such as silicon-on-insulator (SOI) for photonic devices is its sensitivity to dimensional variations. Dimensional deviations of the devices will cause a shift in the spectral response. AWGs are larger in size (few tens of micrometers), which makes them much more vulnerable to different sources of dimensional variations, such as fabrication non-uniformity in the silicon layer thickness, and mask error [12], [13]. An intra-die average non-uniformity of silicon layer thickness ($\sim$0.5 nm) and its strong correlation with the peak wavelength shift (up to $\sim$2 nm) of AWGs have been reported [12].

In this letter, a tunable silicon AWG based on thermo-optic (TO) effect has been demonstrated. By taking advantage of the TO effect in silicon, thermal tuning can be employed to compensate for non-uniformity. The wide ridge-waveguide and the narrow channel-waveguide are designed for reducing the impact of the fabrication non-uniformity. The thermal distribution simulation shows that a uniform heating can be achieved by the heater design, while the experiment results reveal that above 600 GHz channel tunability has been achieved.

II. Design and Fabrication

An eight-channel 400 GHz silicon AWG is designed as the MUX/DeMUX. High-resistivity TiN material is used as heater, while low-resistivity Cu is used as electrode and vias for the purpose of the photonics-CMOS integration [14]. The design parameters are shown in Table I. Since the effective-refractive-index (n_{eff}) related optical performance of silicon AWG is severely sensitive to the fabrication tolerance and non-uniformity as described in introduction section, the following three designs are adopted to reduce the impact of fabrication non-uniformity, and to achieve a uniform heating and tuning.

First of all, the wide straight ridge-waveguide (0.8 μm-rib width) and the narrow bended channel-waveguide (0.5 μm-width) are utilized. One advantage of

Manuscript received July 3, 2015; revised July 23, 2015; accepted July 26, 2015. Date of publication August 3, 2015; date of current version September 30, 2015.

Y. Yang is with the School of Electrical and Electronic Engineering, Nanyang Technological University, Singapore 639798, also with the Institute of Microelectronics, Agency for Science, Technology and Research, Singapore 117685, and also with the Centre National de La Recherche Scientifique, Thales Group, Nanyang Technological University, Singapore 637553 (e-mail: yyang10@e.ntu.edu.sg).

X. Hu and Rusli are with the School of Electrical and Electronic Engineering, Nanyang Technological University, Singapore 639798 (e-mail: huxi0011@e.ntu.edu.sg; erusli@ntu.edu.sg).

J. Song, Q. Fang, M. Yu, X. Tu, and G.-Q. Lo are with the Institute of Microelectronics, Agency for Science, Technology and Research, Singapore 117685 (e-mail: songjf@ime.a-star.edu.sg; fangq@ime.a-star.edu.sg; mingbin@ime.a-star.edu.sg; tux@ime.a-star.edu.sg; logq@ime.a-star.edu.sg).

Color versions of one or more of the figures in this letter are available online at http://ieeexplore.ieee.org.

Digital Object Identifier 10.1109/LPT.2015.2464073

TABLE I
DESIGN PARAMETERS OF THE SILICON AWG

Parameter	Symbol	Value
Central wavelength	λ_0	1.55 μm
Channel spacing	$\Delta\lambda$	3.2 nm
Heater spacing	D_h	4 μm
Heater width	W_h	10 μm
Number of input channels	N_i	1
Number of output channels	N_o	8
Number of arrayed waveguide	N_w	23
Diffraction order	m	50
Path difference	ΔL	28 μm
Free spectral range	FSR	25 nm
Pitch width of arrayed waveguide [15]	d	2.8 μm

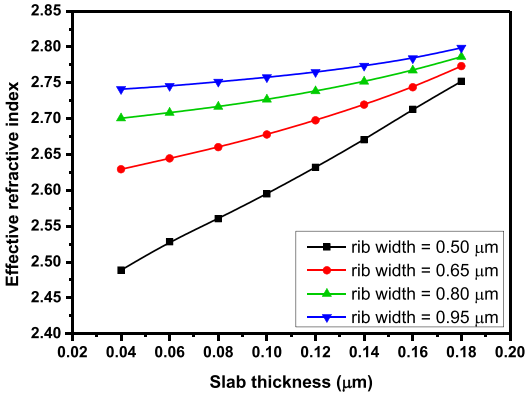

Fig. 1. Simulated effective-refractive-index (n_{eff}) of the ridge waveguide with the different slab thicknesses and rib widths.

the ridge-waveguide is the low optical transmission loss of the straight waveguide under transverse-electric (TE) mode. Another advantage of the wide ridge-waveguide is the small impact of the waveguide thickness (rib thickness and slab thickness) on the waveguide effective-refractive-index (n_{eff}). Furthermore, wide rib dimension is used for reducing the fabrication non-uniformity impact on the waveguide n_{eff}. As shown in Fig. 1, the slab thickness has a smaller impact on the n_{eff} of the ridge-waveguide with a wider rib, as compared to narrower rib. At the same time, a disadvantage of the ridge-waveguide is the high optical transmission loss of the bended waveguide. Bended ridge-waveguide with large radius is one solution to reduce the transmission loss, however, the large device size arising from the bended waveguide with large radius is not beneficial to the integration. Therefore, narrow channel-waveguide is used as the bended waveguide. Taper is used as the transition structure from the narrow channel-waveguide to the wide ridge-waveguide, as shown in inset i of Fig. 4 in section II B Fabrication. Besides, a wide heater (10 μm) is designed with small spacing (4 μm) to achieve a uniform heating on the silicon waveguide. The fold line structure is designed for the heater. To reduce the heater resistance and hence the operating voltage, parallel structure of the left and right part of the heater is designed, as shown in Fig. 4 in section II B Fabrication. In addition, adjacent deep trenches for thermal insulation with other devices are designed around the heater.

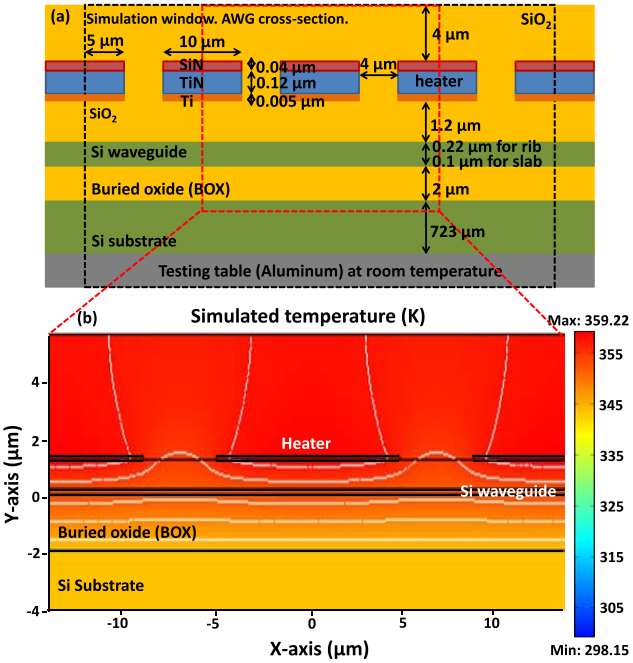

Fig. 2. (a) Thermal simulation structure (not to scale). (b) Simulated cross-sectional thermal distribution when a 40V bias voltage (1.26 W power) is applied to the TiN heater. The temperature of the silicon waveguide is ~53K higher than the room temperature (298.15 K). The white line in the figure is the isothermal line. The simulation image is partially presented.

A. Thermal Performance Simulation and Analysis

To investigate the thermal effect on the device, the cross-sectional thermal distributions under different bias voltages/powers on the TiN heater are simulated by COMSOL Multiphysics commercial software. The thermal conductivity of each material is the important parameter used in the simulation, which measures its ability to conduct heat. Figure 2(a) shows the thermal simulation structure, while Fig. 2(b) shows the simulated result when a 40 V voltage (1.26 W power) is applied to the heater, and the simulation image is partially presented here. The minimum temperature shown in the scale bar is located at the bottom of the silicon substrate, which is not shown in Fig. 2(b). The temperature of the Si waveguide is increased by ~53 K from the room temperature (298.15 K), which will lead to the thermal-induced wavelength shift ($\Delta\lambda$) of the device due to the TO effect. In addition, the simulated temperature of the Si waveguide under different bias voltages/powers with a step of 5 V on the TiN heater is shown in Fig. 3. The result shows that the temperature of the Si waveguide is uniform with a variation of less than 1 K, which ensures the uniform tunability of the device.

The wavelength shift ($\Delta\lambda$) arising from the simulated heating temperature (ΔT) due to the TO effect can be calculated by Eq. (1), Eq. (2) and the TO coefficient of Si/SiO$_2$ ($(dn/dT)_{Si}$ = +1.84e-4/K, $(dn/dT)_{SiO2}$ = +1.0e-5/K).

$$\Delta\lambda = \frac{\Delta n_{eff}}{n_g}\lambda_0 \tag{1}$$

$$\Delta n_{eff} = \frac{\partial n_{eff}}{\partial n_{Si}}\Delta n_{Si} + \frac{\partial n_{eff}}{\partial n_{SiO_2}}\Delta n_{SiO_2} \tag{2}$$

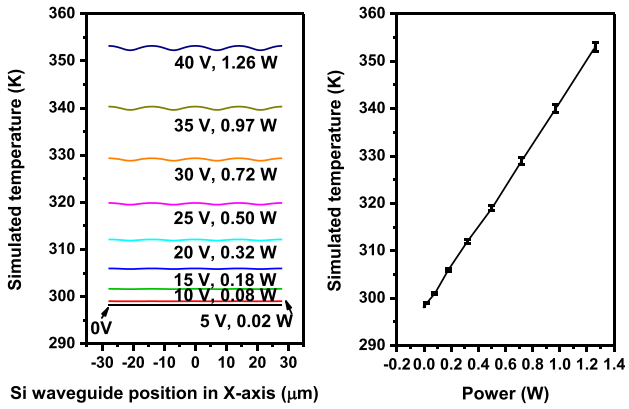

Fig. 3. Simulated temperature distribution of the silicon waveguide under different bias voltages/powers on TiN heater. Less than 1 K temperature variation is observed from the error bar.

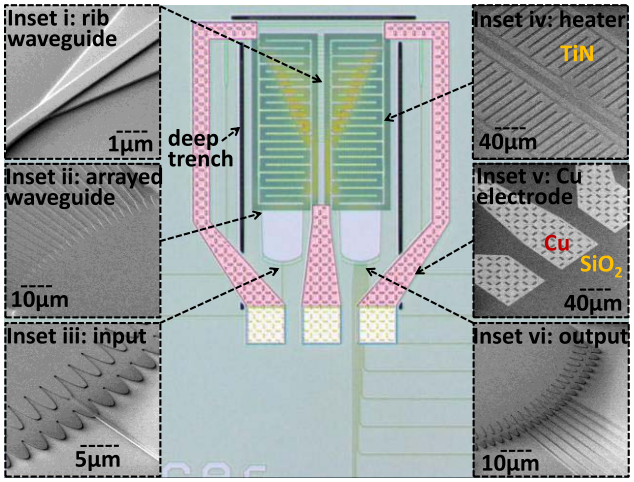

Fig. 4. Microscope image of the tunable silicon AWG. Inset i: SEM image of the rib waveguide. Inset ii: SEM image of the arrayed waveguide. Inset iii: SEM image of the input waveguide. Inset iv: SEM image of the TiN heater. Inset v: SEM image of the Cu electrode. Inset vi: SEM image of 8 channels output.

where n_{eff} denotes the effective-refractive-index of the AWG, n_g denotes the group index, and n_{Si}/n_{SiO2} denotes the refractive-index of Si/SiO_2. The change in n_{eff} of the AWG (Δn_{eff}) is mainly caused by the change in refractive-index of Si (Δn_{Si}) and SiO_2 (Δn_{SiO2}), which is simulated using Mode Solver of Rsoft commercial software. The simulated $\Delta\lambda$ under different voltage/power compared with the measured $\Delta\lambda$ is shown in the Fig. 8 in section III.

B. Fabrication

This tunable AWG was fabricated on an 8-inch SOI wafer with top Si layer of 220 nm and buried oxide (BOX) of 2 μm. The waveguide was formed by double silicon dry etching processes. The microscope image of the tunable AWG is shown in Fig. 4. The insets of Fig. 4 show the scanning electron microscope (SEM) images of the silicon waveguide, heater and Cu electrode. After SiO_2 dielectric layer was deposited and polished, Ti/TiN was deposited and etched as heater. 0.12 μm-thick TiN is used as heater material for its high resistivity, and 5 nm-thick Ti was fabricated underlying the TiN heater for improving the material adhesion to oxide. 0.4 μm-thick SiN deposited above the TiN heater is used as via etching stop layer due to its better etch selectivity.

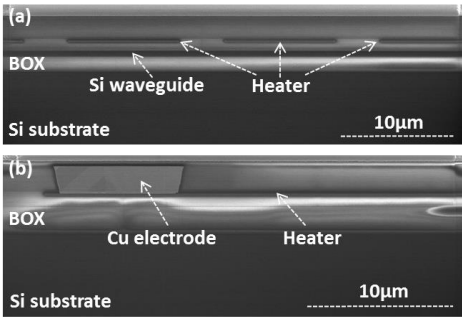

Fig. 5. Cross-sectional SEM images of (a) the heater and the Si waveguide; (b) the Cu electrode and vias to heater.

From the photonics-CMOS integration scenario, Cu was selected as the electrode and vias material. Since it is difficult to delineate Cu by subtractive etch due to the limited number of volatile Cu compounds, dual-damascene process was utilized to form the Cu electrode vias [16]. Cu deposition and chemical-mechanical polishing (CMP) processes are included in dual-damascene process. To avoid the dishing caused by CMP process on Cu surface, a latticed Cu surface pattern is designed [17], as shown in inset v of Fig. 4.

After the SiO_2 dielectric layer was deposited and polished, the trench of Cu electrode and the vias were formed in sequence. To avoid the diffusion of Cu into the Si/SiO_2 layer, a 250 Å-thick TaN barrier layer was deposited first. A 1500 Å-thick Cu seed layer was next deposited by physical vapor deposition (PVD) followed by 6 μm-thick Cu layer by electrochemical-plating (ECP). After removing the excess Cu by CMP, the Cu electrode and vias were finally formed after annealing. The inset v of Fig. 4 shows the SEM image of the Cu electrode surface after Cu CMP. A 5000 Å-thick SiO_2 was deposited as a dielectric layer over the Cu electrode subsequently. After the opening of the bond-pad, a thin Al layer was formed on the bond-pad pattern to avoid the oxidation of Cu electrode. Finally, 120 μm-deep Si trench was etched to hold optical lensed fiber for coupling with the nanotaper of Si waveguide. Other deep trenches were etched also for thermal insulation around the heater, as shown in Fig. 4. Cross-sectional SEM images of the heater, the Si waveguide, the Cu electrode and vias to heater are shown in Fig. 5.

III. Characterization and Discussion

Two lensed fibers with 2.5 μm focal-length were used to characterize the optical performance of this tunable AWG. When the Cu-to-waveguide distance is more than 1 μm, the Cu-induced optical loss is less than 0.25 dB/cm [17]. Compared with the other losses, such as waveguide propagation loss and coupling loss, the Cu-induced propagation loss in our AWG is negligible [17]. The measured output spectra of 8 channels output of the silicon AWG before heating are shown in Fig. 6. The channel spacing is 3.2 nm.

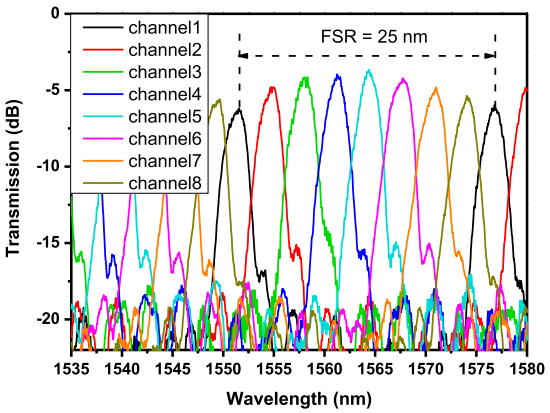

Fig. 6. Transmission of 8 channels output before heating.

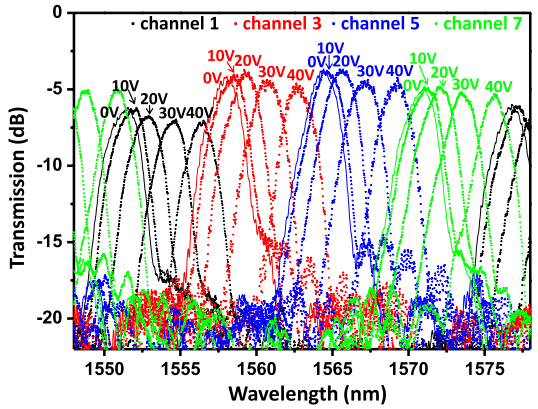

Fig. 7. Transmission of output channel 1, 3, 5 and 7 of the AWG under 0 V (0 W), 10 V (0.08 W), 20 V (0.32 W), 30 V (0.72 W), and 40 V (1.26 W).

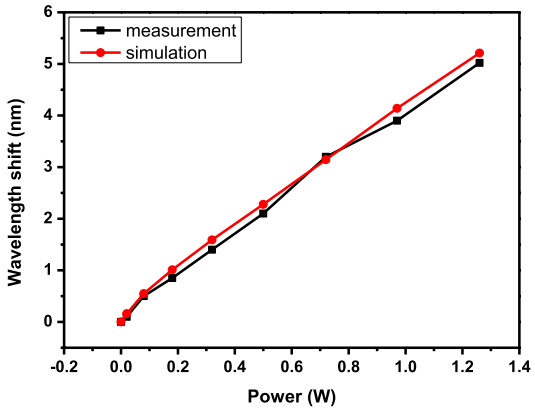

Fig. 8. Measured and simulated wavelength shift under different bias powers.

The optical loss is ∼5 dB. The measured output spectra of four of the 8 channels of the silicon AWG under different bias voltages/powers are shown in Fig. 7. The measure wavelength shifts under different bias powers/powers are shown in Fig. 8, which is in agreement with the simulated wavelength shift. Above 600 GHz channel tunability is achieved. For reducing the power consumption, an optimization method can be utilized. By removing the underlying Si substrate to form a suspended device using SiF_6 etching, the power consumption can be significantly reduced by 98% [18].

IV. Conclusion

A thermo-optically tunable silicon AWG using TiN heater has been demonstrated for the first time. Reduced impact of fabrication nonuniformity on the AWG n_{eff} is achieved through the design of wide ridge-waveguide and narrow channel-waveguide. Uniform heating is achieved by the heater design, which is analyzed by thermal distribution simulation. Above 600 GHz channel tunability has been demonstrated by simulation and experiment.

References

[1] A. R. Vellekoop and M. K. Smit, "Four-channel integrated-optic wavelength demultiplexer with weak polarization dependence," *J. Lightw. Technol.*, vol. 9, no. 3, pp. 310–314, Mar. 1991.

[2] Q. Fang *et al.*, "Monolithic integration of a multiplexer/demultiplexer with a thermo-optic VOA array on an SOI platform," *IEEE Photon. Technol. Lett.*, vol. 21, no. 5, pp. 319–321, Mar. 1, 2009.

[3] C. Dragone, "An N∗N optical multiplexer using a planar arrangement of two star couplers," *IEEE Photon. Technol. Lett.*, vol. 3, no. 9, pp. 812–815, Sep. 1991.

[4] M. E. Vieira Segatto, G. D. Maxwell, R. Kashyap, and J. R. Taylor, "High-speed transmission and dispersion characteristics of an arrayed-waveguide grating," *Opt. Commun.*, vol. 195, nos. 1–4, pp. 151–157, Aug. 2001.

[5] J. Dieckröger, R. März, P. C. Clemens, G. Heise, and H. W. Schneider, "Thermooptically tunable optical phased array in SiO_2/-Si," *IEEE Photon. Technol. Lett.*, vol. 11, no. 2, pp. 248–250, Feb. 1999.

[6] H. Bissessur, F. Gaborit, B. Martin, G. Ripoche, and P. Pagnod-Rossiaux, "Tunable phased-array wavelength demultiplexer on InP," *Electron. Lett.*, vol. 31, no. 1, pp. 32–33, Jan. 1995.

[7] D. H. P. Maat, F. H. Groen, R. C. Horsten, Y. C. Zhu, P. Kruis, and C. Herben, "Tunable phased array demultiplexer and InP featuring wide-range tuning and pass-band shaping," in *Proc. 9th Eur. Conf. Integr. Opt. (ECIO) Postdeadline Papers*, Turin, Italy, Apr. 1999, pp. 25–28.

[8] A. Alonso, J. Stulemeijer, F. Soares, X. Leijtens, and M. Smit, "Electro-optical and temperature tunable WDM filter," in *Proc. IEEE/LEOS Symp. Benelux Chapter*, Enschede, The Netherlands, Nov. 2003, pp. 51–54.

[9] M. Kohtoku, H. Sanjoh, Y. Kadota, and Y. Yoshikuni, "Packaged polarization-insensitive WDM monitor with low loss (7.3 dB) and wide tuning range (4.5 nm)," *IEEE Photon. Technol. Lett.*, vol. 10, no. 11, pp. 1614–1616, Nov. 1998.

[10] H. M. Zhang *et al.*, "Thermo-optically tunable arrayed-waveguide-grating made of polymer/Si," *Optoelectron. Lett.*, vol. 2, no. 4, pp. 243–245, Jul. 2006.

[11] S. Toyoda *et al.*, "Polarization-independent low-crosstalk polymeric AWG-based tunable filter operating around 1.55 μm," *IEEE Photon. Technol. Lett.*, vol. 11, no. 9, pp. 1141–1143, Sep. 1999.

[12] S. K. Selvaraja, W. Bogaerts, P. Dumon, D. Van Thourhout, and R. Baets, "Subnanometer linewidth uniformity in silicon nanophotonic waveguide devices using CMOS fabrication technology," *IEEE J. Sel. Topics Quantum Electron.*, vol. 16, no. 1, pp. 316–324, Jan./Feb. 2010.

[13] S. Pathak *et al.*, "Effect of mask discretization on performance of silicon arrayed waveguide gratings," *IEEE Photon. Technol. Lett.*, vol. 26, no. 7, pp. 718–721, Apr. 1, 2014.

[14] Y. Yang, Q. Fang, M. Yu, X. Tu, J. Song, Rusli, and G. Lo, "High-performance Si photonics interposer featuring RF travelling-wave electrode (TWE) via Cu-BEOL," in *Proc. Opt. Fiber Commun. Conf. (OFC)*, Los Angeles, CA, USA, Mar. 2015, pp. 22–26.

[15] T. Ye, Y. Fu, L. Qiao, and T. Chu, "Low-crosstalk Si arrayed waveguide grating with parabolic tapers," *Opt. Exp.*, vol. 22, no. 26, pp. 31899–31906, Dec. 2014.

[16] R. H. Havemann and J. A. Hutchby, "High-performance interconnects: An integration overview," *Proc. IEEE*, vol. 89, no. 5, pp. 586–601, May 2001.

[17] Y. Yang, Q. Fang, M. Yu, X. Tu, R. Rusli, and G.-Q. Lo, "High-efficiency Si optical modulator using Cu travelling-wave electrode," *Opt. Exp.*, vol. 22, no. 24, pp. 29978–29985, Nov. 2014.

[18] Q. Fang *et al.*, "Ultralow power silicon photonics thermo-optic switch with suspended phase arms," *IEEE Photon. Technol. Lett.*, vol. 23, no. 8, pp. 525–527, Apr. 15, 2011.